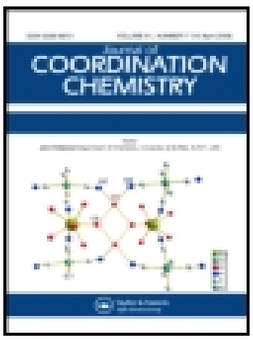

Journal of Coordination Chemistry

ISSN: 0095-8972 (Print) 1029-0389 (Online) Journal homepage: http://www.tandfonline.com/loi/gcoo20

A phenoxo–azido assorted Schiff base copper(II) bridged dimer in trace level fluorescence sensing of a pesticide: a DFT supported phenomenon

Partha Pratim Chakrabarty, Sanjib Giri, Kamalika Sen, Sandip Saha, Atish Dipankar Jana, Santiago García Granda, Shobhraj Haldar & Manindranath Bera

To cite this article: Partha Pratim Chakrabarty, Sanjib Giri, Kamalika Sen, Sandip Saha, Atish Dipankar Jana, Santiago García Granda, Shobhraj Haldar & Manindranath Bera (2016): A phenoxo–azido assorted Schiff base copper(II) bridged dimer in trace level fluorescence sensing of a pesticide: a DFT supported phenomenon, Journal of Coordination Chemistry, DOI: 10.1080/00958972.2016.1223844

To link to this article: http://dx.doi.org/10.1080/00958972.2016.1223844

JOURNAL OF COORDINATION CHEMISTRY, 2016
http://dx.doi.org/10.1080/00958972.2016.1223844

Taylor & Francis
Taylor & Francis Group

A phenoxo–azido assorted Schiff base copper(II) bridged dimer in trace level fluorescence sensing of a pesticide: a DFT supported phenomenon

Partha Pratim Chakrabarty[a,b], Sanjib Giri[a], Kamalika Sen[a], Sandip Saha[b], Atish Dipankar Jana[c], Santiago García Granda[d], Shobhraj Haldar[e] and Manindranath Bera[e]

[a]Department of Chemistry, University of Calcutta, Kolkata, India; [b]Department of Chemistry, Acharya Prafulla Chandra College, Kolkata, India; [c]Department of Physics, Behala College, Kolkata, India; [d]Departamento de Química Físicay Analítica, Universidad de Oviedo, Oviedo, Spain; [e]Department of Chemistry, University of Kalyani, Kalyani, India

ABSTRACT

A binuclear phenoxo- and azido-bridged copper(II) Schiff base complex has been synthesized along with its mononuclear copper-Schiff base analog. The compounds have been characterized by IR spectroscopy and CHN elemental analysis. The single-crystal structure and variable temperature magnetic properties of the binuclear compound have been studied from the X-ray crystallographic data and superconducting quantum interference device magnetometry, respectively. The synthesized crystalline binuclear complex has interesting spectral features that allow it to act as a spectral sensor toward an organophosphorus pesticide which is a potential environmental toxicant coming to the environment as agricultural waste. Although both the mononuclear and binuclear complexes are suitable as sensors for the organophosphorus, the binuclear complex being crystalline is suitable for attaining structural and mechanistic details of the interaction. Density functional theory calculations and ESI MS analysis of the interactions with the binuclear complex suggest that the binding of organophosphorus substrate with **2** occurs through one copper center.

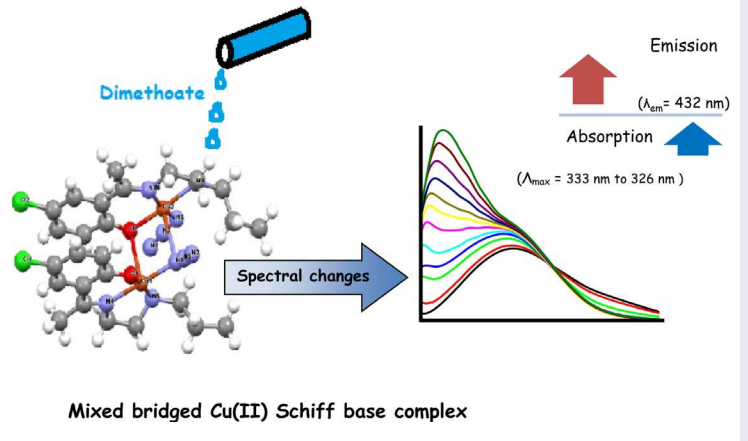

ARTICLE HISTORY
Received 7 November 2015
Accepted 24 June 2016

KEYWORDS
Mixed bridged; Schiff base; copper(II); organophosphorus; sensing; DFT study

CONTACT Kamalika Sen kschem@calunic.ac.in; Sandip Saha sandipsaha2000@yahoo.com
Supplemental data for this article can be accessed at http://dx.doi.org/10.1080/00958972.2016.1223844.

1. Introduction

A huge class of metal Schiff base complexes with myriad structures, particularly those derived from amino and carbonyl functionalities, have been reported owing to their multitude of applications [1]. The ligands in such complexes coordinate to metal ions via azomethine nitrogen wherein the –CH=N– linkage forms the basis of their biological activity that is reflected in their antibacterial, antifungal, anticancer, and diuretic activities [2]. These complexes have applications in analytical chemistry, catalysis, food industry, dye industry, and fungicidal and agrochemical activities [3–6]. Quite a large number of Schiff base complexes are used as model compounds in biological experiments [7]. These compounds play decisive roles in the development of modern coordination chemistry and provide key aspects in development of inorganic biochemistry, catalysis, and optical materials [8]. More recently, their role as chemosensors has developed [9, 10]. We have recently reported the anion sensing property of some heterometallic Schiff base complexes [6].

Organophosphate (OP) pesticides are in extensive use by agricultural industries all over the world. The general chemical structure of these OP compounds consists of a tetra-substituted P(V) center, an oxygen or sulfur double bonded to the phosphorus, a leaving group, and two substituents that vary widely depending on the subclass. A typical OP compound used in our study, *O,O*-dimethyl *S*-[2-(methylamino)-2-oxoethyl]dithiophosphate, is presented in scheme 1. Due to their ubiquitous nature, great environmental concerns have arisen out of this type of pollution. Some of the organophosphorus compounds are lethal to humans at minuscule doses and include some of the most toxic substances ever created by man. Unfortunately, widespread and frequent commercial use of OP-based compounds in agriculture has resulted in their presence as residues in crops, livestock, and poultry products and also resulted in their migration into aquifers. Ideal detection of these compounds at trace concentrations in the environment is not easy as they require expensive mass analyzers (GCMS) which are beyond the reach of many volunteering organizations. The most common ways for detecting OP pesticides are chromatographic methods coupled with different detectors and spectrometry [11, 12]. This method is sensitive and reliable but cannot be carried out in the field and it is expensive and time consuming. Fast, sensitive, and field-deployable screening technology are under consideration for quick response. A variety of approaches have been investigated for designing such sensors, including enzymatic assays [13], molecular imprinting coupled with luminescence [14, 15], colorimetric methods [16], fluorescent organic molecules [17, 18], and enzyme biosensors based on inhibition of cholinesterase activity [19]. Sensor activity based on fluorescence quenching (turn off) methods has been observed more frequently than the "turn on" phenomenon. In most cases, quenching occurs due to non-specific interactions. Fluorescence "turn on" is however rarely observed and when observed is representative of significant molecular interactions [20-24]. Additionally, spectral sensing ability of Schiff base copper complexes was not reported to the best of our knowledge. However, a Cu(II)–cyclen complex was reported to have sensing property toward H_2S [25].

Keeping these practical aspects in mind, herein we report the synthesis of a phenoxo–azido bridged Cu(II) Schiff base dimeric complex together with its mononuclear counterpart. Characterization was done by UV–vis, CHN elemental analysis, IR, and crystal structure together with the chemosensor activity toward trace level detection of organo-phosphate pesticide. The results were further supported by density functional theory (DFT) study.

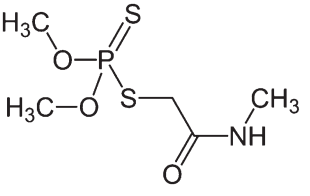

Scheme 1. Dimethoate (*O,O*-dimethyl *S*-[2-(methylamino)-2-oxoethyl]dithiophosphate).

2. Experimental

2.1. Materials and instrumentation

N-propylethylenediamine, 2-hydroxy-5-chloro-acetophenone, copper(II) perchlorate hexahydrate, sodium azide, methanol, and DMSO were purchased from Sigma-Aldrich and used as received. All the chemicals used were of analytical grade. The organophosphorus compound dimethoate was purchased from Sigma-Aldrich. IR spectra were recorded as KBr pellets from 4000 to 400 cm^{-1} on a Perkin-Elmer Spectrum 65 FTIR Spectrometer. Elemental analyses were carried out using a Heraeus CHN-O-Rapid elemental analyzer. Luminescence spectrometer LS-55B (Perkin-Elmer, U.S.A) was used for fluorescence intensity measurements. Horiba Jobin Yvon Fluorocube 01-NL and 291 nm Horiba nanoLED, IBH *DAS-6* decay analysis software were used for Time-Correlated Single Photon Counting Lifetime Spectroscopy. The UV–vis spectra were obtained using an Agilent 8453 diode array spectrophotometer. Total independent data for **2** were collected on a Bruker Smart Apex II CCD Area Detector equipped with graphite monochromated Mo K_α radiation (λ = 0.71073 Å). Theoretical calculations were carried out using Gaussian 03 software. All the ESI-MS spectra were recorded in a WATERS Xevo G2-SQTof. NMR spectra were obtained on a 500 MHz Bruker spectrometer using $CDCl_3$ solvent. Temperature-dependent molar susceptibility for powdered sample of **2** was measured with a superconducting quantum interference device vibrating sample magnetometer (Quantum Design) with an applied field of 1000 Oe from 2 to 300 K.

2.2. Syntheses

Caution! Since metal azides and perchlorates are potentially explosive, only small amount of the material should be prepared and handled with care.

To a solution of 2-hydroxy-5-chloro-acetophenone (2 mmol, 340 mg) in 20 mL methanol, N-propylethylene diamine (2 mmol, 204 mg) was added dropwise and the resulting mixture was heated under reflux for 4 h. The ligand was thus prepared by 1 : 1 condensation of the two components in methanol. A methanolic solution of $Cu(ClO_4)_2{\cdot}6H_2O$ (2 mmol, 730 mg) was then added and the mixture was refluxed for another 2 h to obtain a deep-green solution. Complex **1** was obtained after slow evaporation of this green solution. The aqueous solution of NaN_3 (4 mmol, 260 mg) dissolved in minimum volume of water was then added dropwise to the green solution of **1**. Then the resulting mixture was stirred for about another 2 h and was filtered. The greenish solution was kept at room temperature for seven days. Black needle-shaped crystals of the product (**2**) were obtained.

2.2.1. ^{1}H NMR spectroscopy of the synthesized ligand

500 MHz, $CDCl_3$, 298 K, ppm: δ 0.746 (t, 2H, $-CH_2CH_2CH_3$); 1.122 (m, 2H, $-CH_2CH_2CH_3$); 2.054 (s, 3H, $-CH_3$ of imine); 2.511 (t, 2H, $-CH_2CH_2CH_3$); 3.122–3.999 (m, 4H, $-CH_2CH_2-$ of ethylene diamine); 4.825 (s, 1H, –OH); 6.834–7.611 (m, 3H, ring) (figure S1).

2.2.2. Complex **1**

$[Cu(L^{-1}).CH_3OH]^+ClO_4^-$: yield 80% (0.511 g). Anal. Calcd for $C_{14}H_{20}Cl_2CuN_2O_6$: C, 37.6; H, 4.5; N, 6.3. Found: C, 38; H, 4.6; N, 6.1%. IR (KBr pellets, cm^{-1}): $\nu(CH_3OH)$ 3467, $\nu(C{=}N)$ 1602, $\nu(ClO_4)$ 1097.

2.2.3. Complex **2**

Yield 70% (0.357 g). Anal. Calcd for $C_{26}H_{34}Cl_2Cu_2N_{10}O_2$: C, 43.5; H, 4.7; N, 19.9. Found: C, 44.0; H, 4.9; N, 19.1%. IR (KBr pellets, cm^{-1}): $\nu(N_3)$ 2044, $\nu(C{=}N)$ 1600, ESI MS (*m/z*): 674.08 (Calcd 674 for $[C_{26}H_{34}Cl_2Cu_2N_7O_2]^+$).

2.3. OP sensing studies using spectral methods

0.1 mmol solution of **1** (ligand + Cu) and 0.1 mmol solution of **2** (ligand + Cu + azide) in DMSO were prepared for absorption and fluorescence spectroscopic measurements. Aliquots of 0.01 mL of dimethoate

Table 1. Crystallographic data for **2**.

Crystal data	Complex **2**
Empirical formula	$C_{26}H_{34}Cl_2Cu_2N_{10}O_2$
Formula weight	716.61
Crystal dimension (mm)	$0.56 \times 0.25 \times 0.13$
Crystal system	Monoclinic
Space group	P 21/n
a (Å)	17.743(4)
b (Å)	7.6735(12)
c (Å)	24.453(4)
α (°)	90.00
β (°)	113.34(2)
γ (°)	90.00
V (Å^3)	3057.0(10)
Z	4
Temperature (K)	293(2)
D_{calcd} (g cm^{-3})	1.557
μ (mm^{-1})	3.679
F(0 0 0)	1472
θ (°)	3.79–70.90
Total data	5692
Unique data	1875
[a]R_1	0.2018
[a]wR_2	0.2409
Goodness-of-fit on F^2, S	0.878
R_{int}	0.0745

[a]Corresponds to all the diffraction data.

(10% v/v in DMSO) were added to the above solutions and the changes in the spectral behavior were recorded.

2.3.1. Time-correlated single photon counting lifetime spectroscopy

The fluorescence lifetimes for **1**, **2,** and the OP-treated complexes were measured by time-correlated single-photon counting using a nanosecond diode laser as the light source at 375 nm. The mean fluorescence lifetimes for each of the curves were calculated from the decay times (τ_i) using the following equation:

$$\tau_{av} = \frac{\Sigma a_i \tau_i^2}{\Sigma a_i \tau_i}$$

where τ_{av} represents the average decay time and a_i represents the coefficient of the ith component. The average lifetimes of all complex species were identified and compared.

2.4. X-ray crystallography of **2**

Crystal data for **2** are given in table 1 and bond distances and angles are in table 2. The structure of **2** was solved by SIR 97 [26]. The structure refinement was also performed by full-matrix least-squares based on F^2 with SHELXL-97 [27]. All non-hydrogen atoms were refined anisotropically. The C–H atoms were constrained to ideal geometry and were included in the refinement in the riding model approximation. Data for molecular geometry, intermolecular interactions, and pictures were produced using Platon-2009 [28] and ORTEP3.2 [29] programs.

Table 2. Selected bond distances (Å) and angles (°) for **2**.

Bond	Distance (Å)	Bond angle	(°)
Cu1–N1	1.98(1)	Cu1–N1–N2	119.0(8)
Cu1–N4	1.96(1)	Cu2–N1–N2	117.0(8)
Cu1–N5	2.046(9)	Cu1–N1–Cu2	94.1(4)
Cu1–O1	1.877(8)	N1–Cu1–N5	92.8(4)
Cu2–N1	2.66(1)	N1–Cu1–O2	83.9(4)
Cu2–N6	1.97(1)	N1–Cu2–O2	84.2(3)
Cu2–N9	2.03(1)	N9–Cu2–O2	175.7(4)
Cu2–O2	1.895(9)	N10–Cu2–O2	91.8(4)
		N1–Cu1–N4	177.6(4)
		N1–Cu1–O1	90.4(4)
		O1–Cu1–O2	106.8(3)

2.5. DFT study and computational methodology

Theoretical calculations regarding structure optimization and Fukui function (f_k^+) of the copper sites of **2** were carried out using Gaussian 03 software [30]. The functions (f_k^+) were estimated from single-point calculations using the B3LYP [31, 32] method and 6-311G [33] basis set at the optimized geometry, performed for N and (N + 1) electron systems, where N is the total number of electrons in the system. In a finite difference approximation, f_k^+ of an atom k, in a molecule with N electrons, is expressed by the equation $f_k^+ = [q_k(N) - q_k(N + 1)]$, where q_k is the charge of atom k [34]. The q_k values were calculated by Mulliken population analysis.

2.6. Mass spectral analysis

For ESI (Electrospray Ionization) mass spectral analysis, the samples were prepared in acetonitrile in the concentration range ~10 µM. Since the XRD data could be obtained for **2** only (being crystalline), an idea about the exact molecular structure and mass of the compound was utilized as a prerequisite to study the molecular interactions between **2** and the OP in our study. Consequently, measurements were performed for **2** and OP-treated **2**. The sample solutions were infused into the ESI source at a flow rate of 10 µL min^{-1}. The electrospray voltage was 3.5 kV and capillary temperature was 110 °C. The lockspray flow rate was 5.0 µL min^{-1}. All the spectra were recorded in the positive mode and the scan time was recorded in the *m/z* range 100–1200 Da.

3. Results and discussion

In the present work, the ligand reacted with copper(II) perchlorate hexahydrate for preparation of **1** and **1** reacts with sodium azide in methanol–water mixture in refluxing condition to prepare dinuclear **2**. Complex **1** was characterized by IR spectroscopy and CHN elemental analysis.

3.1. IR spectroscopy

In the IR spectrum of **1**, a distinct band at 1602 cm^{-1} and a broad band at 3467 cm^{-1} are due to azomethine group and methanol coordinated to copper(II) present in **1**, respectively. A sharp peak at 1097 cm^{-1} is indicative for the presence of perchlorate in the outer sphere of this complex for charge neutralization of copper(II). As there is no splitting of this band, it is indicative of the non-coordination of the perchlorate to copper(II) [35].

In the IR spectrum of **2,** the distinct band observed at 1600 cm^{-1} is due to azomethine (CH=N) of the Schiff base present in the complex. The asymmetric stretching vibration of azide (ν_{as}) is at 2044 cm^{-1} and attributed to end-on azide bridge in **2**. Out of the two complexes, only **2** was found in the crystalline state; structural detail is described below.

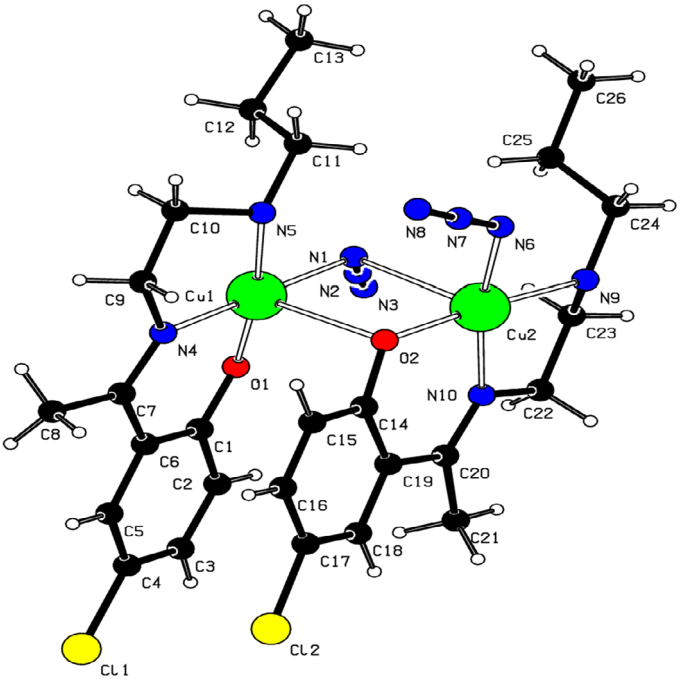

Figure 1. Structure of **2** with atom numbering scheme.

3.2. X-ray crystallography of 2

In this complex, copper(II) centers are held by bridging phenoxo- and bridging $\mu_{1,1}$-N_3 forming the mixed-bridged binuclear species. The binuclear nature is shown in figure 1. The Cu···Cu internuclear distance is 4.395 Å for **2**. Both copper ions have distorted five-coordinate geometry. In the coordination environment of one Cu(II), the basal plane is composed of three nitrogen donors and one oxygen atom, one nitrogen is from the bridging azide (N1), and the other two are from the Schiff base (N4 and N5). The remaining coordination position is occupied by the phenoxo oxygen of tridentate Schiff base (O1). The fifth coordination site of the square pyramid is occupied by O2 of the symmetry-related bridging phenoxo group (symmetry: $1/2 - x, 1/2 + y, -z$). In the coordination environment for the other Cu(II) center, the four coordination sites are similar to the first but one of the coordination sites is occupied by N6 from the terminal azido group. This inequality in coordination environment of the copper(II) centers of the dimer indicates that non-identical copper(II) ions are present in the same fragment. All the bond angles and lengths agree very closely with previously reported phenoxo–azido-bridged copper(II) complexes [36, 37]. The Cu1–O2–Cu2 angle is 102.30(7)° and the Cu1–N1–Cu2 angle is 94.1(4)°.

A closer look into the supramolecular assembly reveals that adjacent dinuclear units are aligned along the crystallographic *b*-axis. A number of weak forces are responsible for this 1-D assembly as shown is figure S2. Cu1 of one unit is at 3.772 Å from the coordinated N6 of the adjacent unit. Similarly a weak N···O interaction is present with O1···N9 distance of 3.006 Å [38]. Cu2 is at a distance of 3.711 Å from O1 which is coordinated with Cu1 of the adjacent unit. Finally a $\pi\cdots\pi$ interaction between the phenyl ring (consisting of C1–C2–C3–C4–C5–C6) and the metal chelate ring (consisting of Cu2–O2–C14–C19–C20–N10) with a centroid···centroid distance of 3.788 Å is also operating between the adjacent dinuclear units. The packing of the complex is depicted in figure S3. In the *ac* plane, the molecular assembly is controlled by van der Waals cohesion among the $-CH_2CH_2CH_3$ aliphatic ends of adjacent dinuclear units. As shown in figure S3, the H···H close contact along the *a*-axis is 3.002 Å and that along the *c*-axis is 2.988 Å [39].

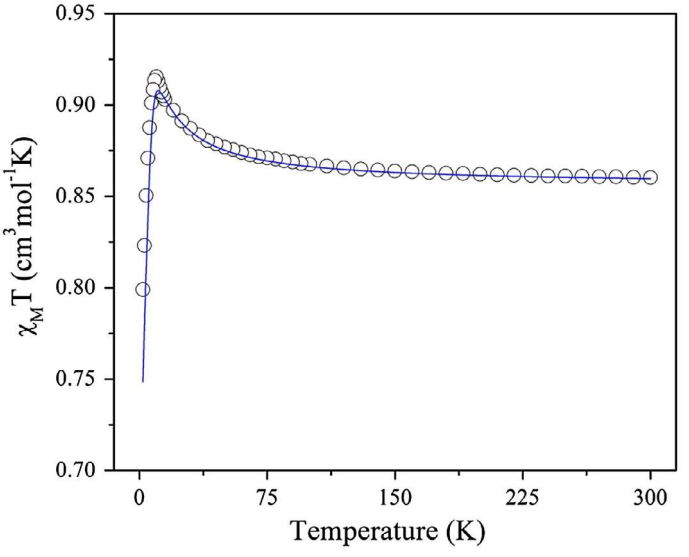

Figure 2. Variation of $\chi_M T$ (cm^3 mol^{-1} K) with temperature for **2**. Solid line denotes the best fitted theoretical curve and the points are the experimental data.

3.3. Magnetic study of **2**

Temperature dependence $\chi_m T$ of **2** is shown in figure 2. The room temperature $\chi_m T$ value is 0.86 cm^3 K mol^{-1}, expected for two magnetically isolated Cu(II) ions with respect to the spin-only value of 0.75 cm^3 K mol^{-1}. As the temperature is lowered, $\chi_m T$ increases slowly to *ca.* 75 K, then sharply increases to a maximum of 0.91 cm^3 K mol^{-1} at 10 K. Upon further cooling, it decreases rapidly and attains a value of 0.79 cm^3 K mol^{-1} at 2 K. This curve is characteristic of leading ferromagnetic interaction. It should be noted that the rapid lowering of $\chi_m T$ at very low temperature might be the effect of antiferromagnetic inter-dimeric interaction. To calculate the exchange coupling (*J*), the data were fitted with a modified Bleaney–Bowers equation [40, 41] (equation 2) for two interacting Cu(II) ions (S = 1/2) taking the Hamiltonian H = $-JS_1S_2$ ($S_1 = S_2 = 1/2$). The modification was done by introduction of the molecular field approximation to incorporate intermolecular interaction. The best fitted curve (figure 1) results in the following parameters: $g = 2.13$, $J = 5.55$ cm^{-1}, $ZJ' = -0.12$ cm^{-1}, and $r = 0.985$. Here, r represents the goodness of fit.

$$\chi_m^{dimer} T = \frac{2Ng^2\beta^2 T}{k(T-\theta) \times \left[3 + \exp(-J/kT)\right]} \tag{1}$$

$$\chi_m^{total} T = \frac{\chi_m^{dimer}}{\left[1 - \left\{\frac{2zJ' \chi_m^{dimer}}{Ng^2\beta^2}\right\}\right]} \tag{2}$$

The structural analysis of **2** shows that each dimeric unit is connected through hydrogen bonds of phenoxido O1 and N9 of adjacent amine group, forming a 1-D chain through weak atom···atom interactions. The donor-acceptor distance is 3.005 Å. Therefore, antiferromagnetic inter-dimer interaction is quite reasonable and expected for this complex. Magnetic exchange pathway between the *axial–equatorial* (*a–e*) positions of copper center always provides weak interaction which may be either ferro or antiferromagnetic depending upon the bridging angle and the nature of bridging group [42]. It is also noticed that weak interaction is caused by a poor overlap of magnetic orbitals since the spin distributed

in the equatorial plane and each copper center possesses two different planes. The molecular structure of **2** shows that Cu–N_{azido} (*equatorial*) bond distance (1.981 Å) is shorter than Cu–N_{azido} (*axial*) bond distance (2.655 Å). Similarly, the Cu–$O_{phenoxido}$ bond distances for equatorial and axial bond are 1.895 and 2.609 Å, respectively. The Cu–(μ1,1–N_3)–Cu and Cu–($O_{phenoxido}$)–Cu bridging angles are 94.14° and 97.75°, respectively. After comparison with previously reported magneto-structural correlations, we can conclude that **2** became ferromagnetic because of low azide bridging angle (~94°) [42]. Besides that, the phenoxido group might show a counter complementarity effect which provides an overall moderate ferromagnetic interaction [42].

3.4. Electronic spectra

The absorption spectrum of the ligand showed bands at 220, 330, and 403 nm which are assigned to $\pi \rightarrow \pi^*$ and $n \rightarrow \pi^*$ transitions arising out of the conjugated double bond and the phenyl ring of the ligand (figure 3). The absorption spectrum of the mononuclear Cu-complex of **1** shows a single band at 330 nm which is diminished in intensity as compared to the ligand itself. This may be attributed to the rigid molecular frame of the copper bound complex that results in $\pi \rightarrow \pi^*$ transition within the aromatic ring and the azomethine group in a restricted way. Complex **2** however shows a red-shift in the band position which is intensified at 334 nm owing to azide bridging between two Cu ions present in two units of **1** [43, 44].

3.5. OP sensing studies

Complexes **1** and **2** were treated separately with OP and studied for their spectral responses. Figure 4 shows a gradual red-shift in the λ_{max} of the absorption spectrum (from 330 to 340 nm and 287 to 300 nm) of **1** upon addition of OP. This is attributed to the higher polarity of the OP compound originating out of the lone pairs on N and S. The $\pi \rightarrow \pi^*$ transition is facilitated with the lowering of the excited state of the complex upon interaction with these lone electron pairs associated with OP. A spectacular change is seen when **2** is treated with OP (figure 5). The absorption spectrum of **2** shows a slight blue-shift (333 to 326 nm) which is due to interaction of the azide bridge with the lone electron pairs of OP that influences the energy involved with the $n \rightarrow \pi^*$ transition. The red-shift in the $\pi \rightarrow \pi^*$ transition however

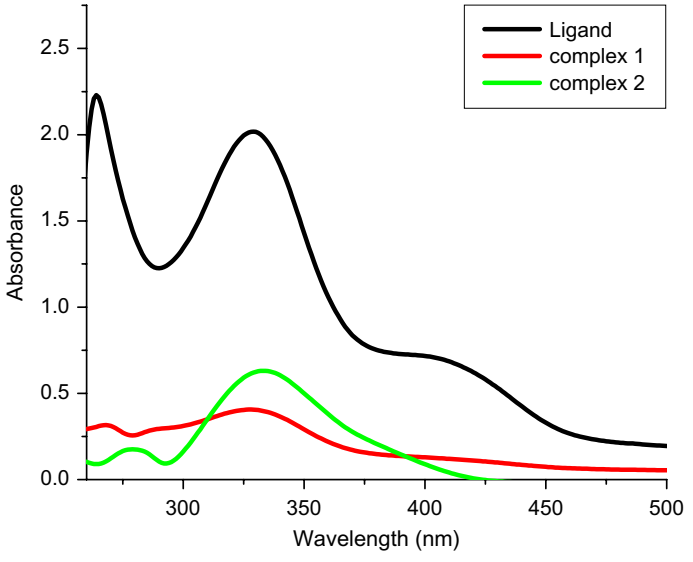

Figure 3. Absorption spectra of the Schiff base, **1** and **2**.

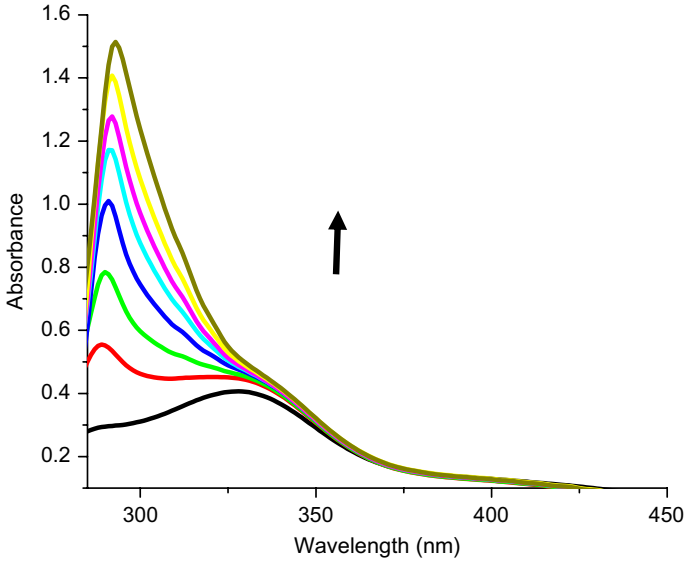

Figure 4. Absorption spectra of **1** with increasing OP concentration from 3.9×10^{-4}–2.7×10^{-3}%.

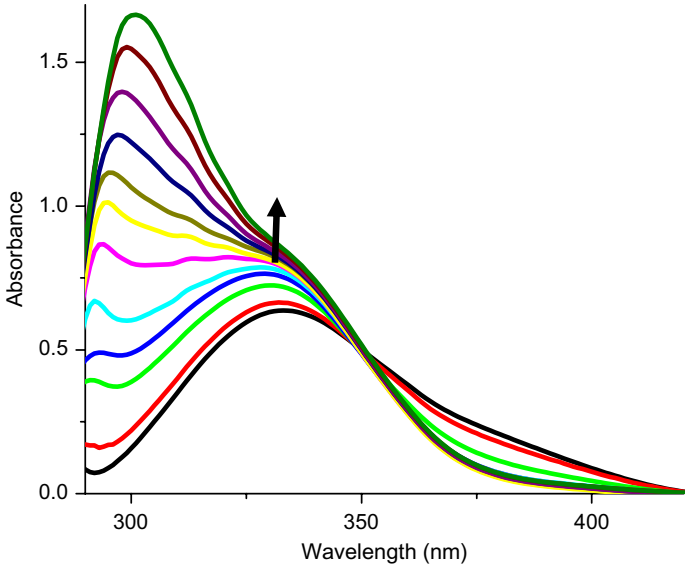

Figure 5. Absorption spectra of **2** with increasing OP concentration from 3.9×10^{-4}–5.6×10^{-3}%.

remains the same as in the previous case. The simultaneous red-shift in the $\pi \rightarrow \pi^*$ and blue-shift in the $n \rightarrow \pi^*$ transition may result in overlapping of the two bands. After addition of only 0.00196% OP in solution of **2**, a considerable overlap of the two peaks is observed. Both absorption and fluorescence spectra of the pristine OP compound taken in DMSO were measured at the same concentration level and found to have no characteristic bands. Considering the possible interference from sulfate, nitrate, and phosphate ions in detection of OP compounds, the changes in the absorbance of **1** and **2** solutions were studied in presence of these ions (figures S4 and S5, respectively). Absence of any considerable change at λ_{max} = 330 nm for **1** and at λ_{max} = 334 nm for **2** nullifies the possibility of interference from these ions in detection and sensing of OP compounds.

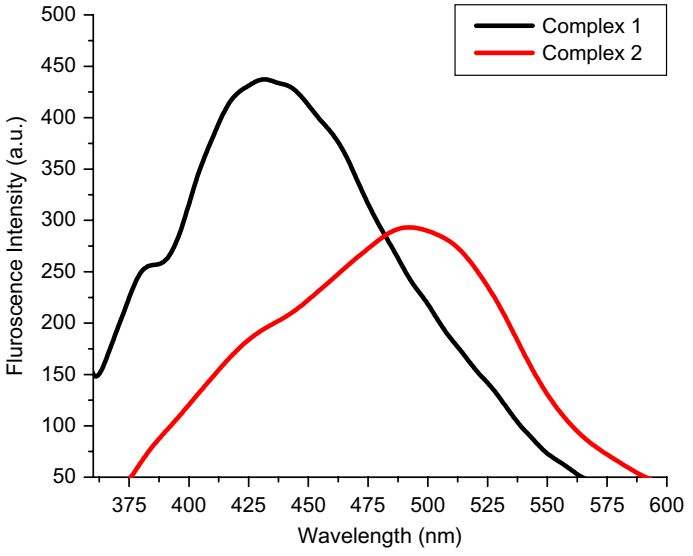

Figure 6. Fluorescence spectra of **1** and **2** excited at 330 nm.

Both **1** and **2**, when dissolved in DMSO, show emission spectra upon excitation at 330 nm (figure 6). A double-humped emission pattern in both complexes is indicative of the existence of a low energy state very close to the ground-state. The emission spectrum was recorded from 320 to 600 nm. Complex **1** shows an emission band with maximum at 434 nm together with a hump at 383 nm. The azide-bridging induces a considerable red-shift in the emission spectrum and **2** emits at 491 nm together with a shoulder at 432 nm, when excited at 330 nm. As a result of azide-bridging between the two adjacent Cu complexes, the distance between the two electron-rich zones of the ligand-bound Cu centers become less and is now almost fixed as compared to the previous situation. This gives decrease in the emission intensity and emission energy. Hence a prominent red-shift is seen in the emission spectrum of **2**.

Addition of the OP solution at a trace level (down to ~0.00039% solution in DMSO) induces a spectacular blue-shift in the emission spectrum of **1** (figure 7). Presence of electronegative O and N together with S-donor atoms imparts changes in the local electronic environment of the Cu complex which results in increased difference in the energy levels of the electrons and, hence, a blue-shift in the emission spectrum. This is in accord with the corresponding absorption spectrum which shows a red-shift upon addition of OP. The two results are in agreement and the absorption and the emission spectra are supposed to be the mirror image of one another.

Addition of OP solution to **2** also shows a prominent change in its emission spectrum (figure 8). With increasing OP concentration, the initial sharp emission band of 491 nm becomes broad and the emission shoulder at 432 nm slowly intensifies resembling the emission maximum (~434 nm) of the OP-treated **1**. This is probably due to slow rupture of the azide bridge upon treatment with OP and a slow conversion of the structure toward that of **1** (figure 6). For further confirmation of the event, the fluorescence lifetimes of the compounds were studied. The fluorescence decay plots are shown in figure S6 showing that the fluorescence decay pattern of **1** varies widely as that in **2**. However, the decay pattern of the OP-treated **2** overlaps with that of **1**, indicating the probable conversion as discussed above. In addition, no observable change in the OP-treated **1** also indicates only excited state interactions with the OP in this particular case. The fluorescence lifetime values (τ) of the compounds as tabulated in table 3 also show that one of the components (τ_2) of the OP-treated **1** now closely resembles that of **1** (5.8 ns). The spectral results are in agreement with each other. The fluorescence sensing of OP compound is due to its possible role in nullifying the azide bridge which is reflected in the resultant absorption and fluorescence spectral behavior.

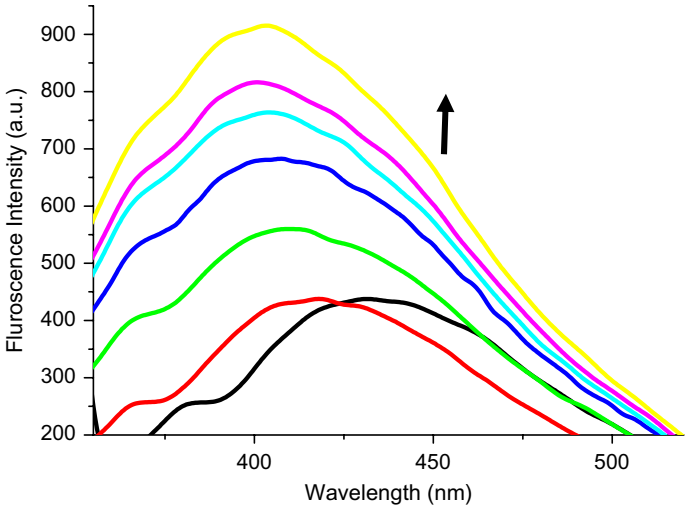

Figure 7. Fluorescence spectra of **1** with increasing OP concentration from 3.9×10^{-4}–2.3×10^{-3}%.

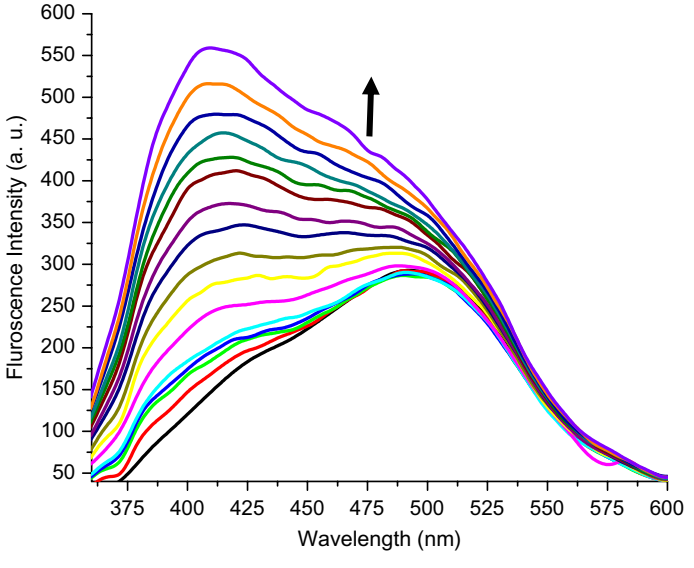

Figure 8. Fluorescence spectra of **2** with increasing OP concentration from 3.9×10^{-4}–5.3×10^{-3}%.

Table 3. Fluorescence lifetimes (in s) of the compounds.

Compound	τ_1	τ_2	τ_3
Ligand	2.01×10^{-9}	6.28×10^{-9}	5.06×10^{-10}
Complex **1**	1.42×10^{-9}	5.80×10^{-9}	1.98×10^{-10}
Complex **2**	1.12×10^{-9}	7.39×10^{-9}	6.88×10^{-11}
Complex **2** + OP	1.24×10^{-9}	5.88×10^{-9}	7.81×10^{-10}

3.6. DFT study

Since a crystal structure was obtained only for **2**, DFT calculations could be done only for this compound to get a better understanding of the binding events between **2** and organophosphorus substrate.

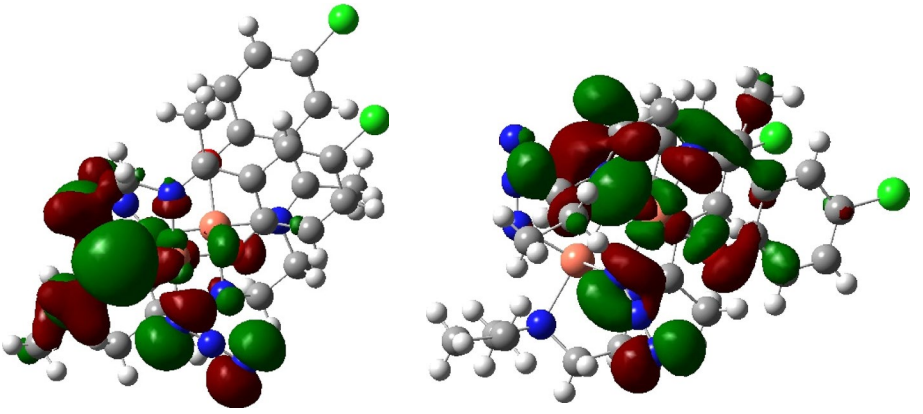

Figure 9. Representative HOMO and LUMO of **2** calculated at the B3LYP/[6-311G] level of theory.

Calculations were performed on **2** and on the corresponding one-electron reduced analog (**1**$^{-}$) at the B3LYP level. The structure of **2** proved to be the triplet (S = 1/2) state with optimized structural parameters fully consistent with crystallographic data. The one-electron reduced analog (**1**$^{-}$) shows a doublet (S = 1/2) ground state. The calculated condensed Fukui function values f_k^+ at the copper sites of **2** are 0.0279 (Cu1) and 0.0180 (Cu2). According to these values, the organophosphorus substrate binds as a nucleophile to one copper center ($f_k^+ = 0.0279$) more favorably compared to the other copper center ($f_k^+ = 0.0180$) in **2**. The difference in Fukui function values at the two copper sites is most likely due to the different modes of ligand coordination. In **2**, both HOMO and LUMOs are spread on and around Cu1, indicating involvement of this copper center in the binding process with the substrate (figure 9(a) and (b)). This is in accord with the findings observed in Fukui function calculations. Similarly, in one-electron reduced analog (**1**$^{-}$), the HOMO and LUMOs are mostly located on Cu1 rather than Cu2. Therefore, DFT calculation results suggest that the binding of organophosphorus substrate with **2** occurs through one copper center.

3.7. ESI-MS study

The interactions were further supported by the ESI-MS analysis of **2** and its OP-treated analog. The spectrum for **2** (figure S7a) shows prominent peaks at *m/z* values 676, 634, and 316 Da, owing to the disappearance of the end on bridging N_3^-, N_3^- and one of the ligand bound copper units, respectively. Upon treatment with OP, the intensity of the peaks at 676 and 634 Da diminish (figure S7b) with respect to that of 316 Da indicating the presence of higher concentration of the mononuclear species which is also in agreement with the fluorescence lifetime data. In addition, a small new *m/z* peak arises at 544.9 Da, which corresponds to the mass of the OP-added mononuclear Cu unit. A zoom in spectrum (figure S7c) of the OP-treated complex **2** shows the presence of the peak at 544.9 Da. However, no such specific peak is seen for pristine **2** (figure S7d), indicating the specificity of the studied interaction. However, some non-specific fragmentations do occur yielding mass fractions of 570, 572 Da, *etc*.

4. Conclusion

An application of a newly synthesized phenoxo–azido-bridged Schiff base complex has been explored. Both the synthesized mononuclear and azido-bridged binuclear complexes were effective

in fluorescence sensing of an organo-phosphorus insecticide which otherwise needs sophisticated method for detection and analysis. Trace concentration of OP solution in DMSO can modify the spectral features of the Schiff base complex containing Cu as the central ion and two Cu Schiff base units bridged with azide. However, sensing by **1** is due to excited-state electronic interactions with the OP molecule in contrast to the ground state electronic interactions of the same with **2**. The observations are in agreement with single X-ray crystallographic features of **2** which have been further supported by theoretical calculations and ESI-MS analysis. The results may offer an economical method for detection of this highly toxic non-biodegradable ingredient in agricultural products.

Supplementary material

Crystallographic data for **2** has been deposited at the Cambridge Crystallographic Data Center (CCDC). CCDC No. of **2** is 1403818. Copy of the data can be obtained free of charge on application to the CCDC, 12 Union Road, Cambridge CB2 1EZ, UK (Fax: +44 1223 336 033; E-mail: deposit@ccdc.cam.ac.uk or http://www.ccdc.cam.ac.uk/conts/retrieving.html).

Acknowledgments

S. S. thankfully acknowledges UGC and DST, New Delhi for funding of the total work done in the Dept. of Chemistry, A. P. C. College. S. S. also acknowledges DST-FIST for funding of Instruments. K. S. acknowledges UGC (Sanction no. 41-248/2012 (SR)) and UGC CAS V for funding.

Disclosure statement

No potential conflict of interest was reported by the authors.

Funding

This work was supported by University Grants Commission [grant number 41-248/2012 (SR)]; University Grants Committee [grant number CASV].

References

[1] P.A. Vigato, S. Tamburini. *Coord. Chem. Rev.*, **248**, 1717 (2004).
[2] D. Sinha, A.K. Tiwari, S. Singh, G. Shukla, P. Mishra, H. Chandra, A.K. Mishra. *Eur. J. Med. Chem.*, **43**, 160 (2008).
[3] K. Singh, M.S. Barwa, P. Tyagi. *Eur. J. Med. Chem.*, **41**, 1 (2006).
[4] M.J. Gemi, C. Biles, B.J. Keiser, S.M. Poppe, S.M. Swaney, W.C. Tarapley, D.L. Romeso, Y. Yage. *J. Med. Chem.*, **43**, 1034 (2000).
[5] T. Maity, D. Saha, S. Bhunia, P. Brandão, S. Das, S. Koner. *RSC Adv.*, **5**, 82179 (2015).
[6] P.P. Chakrabarty, S. Saha, K. Sen, A.D. Jana, D. Dey, D. Schollmeyer, S.C. García-Granda. *RSC Adv.*, **4**, 40794 (2014).
[7] K.S. Suslick, T.J. Reinert. *J. Chem. Educ.*, **62**, 974 (1988).
[8] J. Tisato, F. Refosco, F. Bandoli. *Coord. Chem. Rev.*, **135**, 325 (1994).
[9] A. Ramdas, V. Sathish, M. Velayundhan, P. Thanasekaran, S. Umapathy, S. Rajagopal. *RSC Adv.*, **5**, 98479 (2015).
[10] J. Wu, W. Liu, J. Ge, H. Zhang, P. Wang. *Chem. Soc. Rev.*, **40**, 3483 (2011).
[11] Y. Zhang, Y. Zhang, Q. Qu, G. Wang, C. Wang. *Anal. Methods*, **5**, 6465 (2013).
[12] F. Hernández, J.V. Sancho, O. Pozo. *J. Anal. Bioanal. Chem.*, **382**, 934 (2005).
[13] W. Tang. *Anal. Methods*, **6**, 924 (2014).
[14] A.L. Jenkins, R. Yin, J.L. Jensen. *Analyst*, **126**, 798 (2001).
[15] H. Li, Y. Li. *Chem. Mater.*, **22**, 2451 (2010).
[16] K.J. Wallace, J. Morey, V.M. Lynch, E.V. Anslyn. *New J. Chem.*, **29**, 1469 (2005).
[17] I. Walton, M. Davis, L. Munro, V.J. Catalano, P.J. Cragg, M.T. Huggins, K.J. Wallace. *Org. Lett.*, **14**, 26869 (2012).
[18] S.W. Zhang, T.M. Swager. *J. Am. Chem. Soc.*, **125**, 3420 (2003).
[19] G.A. Evtugyn, H.C. Budnikov, E.B. Nikolskaya. *Analyst*, **121**, 1911 (1996).
[20] Y. Ding, Y. Tang, W. Zhu, Y. Xie. *Chem. Soc. Rev.*, **44**, 1101 (2015).
[21] Y. Xie, P. Wei, X. Li, T. Hong, K. Zhang, H. Furuta. *J. Am. Chem. Soc.*, **135**, 19119 (2013).
[22] Y. Ding, X. Li, T. Li, W. Zhu, Y. Xie. *J. Org. Chem.*, **78**, 5328 (2013).
[23] B. Chen, Y. Ding, X. Li, W. Zhu, J.P. Hill, K. Ariga, Y. Xie. *Chem. Commun.*, **49**, 10136 (2013).
[24] Y. Ding, Y. Xie, X. Li, J.P. Hill, W. Zhang, W. Zhu. *Chem. Commun.*, **47**, 5431 (2011).

[25] H. Wu, S. Krishnakumar, J. Yu, D. Liang, H. Qi, Z.W. Lee, L.W. Deng, D. Huang. *Chem. Asian J.*, **9**, 3604 (2014).
[26] A. Altomare, M.C. Burla, M. Camalli, G.L. Cascarano, C. Giacovazzo, A. Guagliardi, A.G.G. Moliterni, G. Polidori, R. Spagna. *J. Appl. Cryst.*, **32**, 115 (1999).
[27] G.M. Sheldrick. *SHELXTL, Version 5.1, Program for the Solution and Refinement of Crystal Structures*, Bruker AXS Inc., Madison, Wiskonsin, USA (1999).
[28] A.L. Spek. *Acta Cryst.*, **D65**, 148 (2009).
[29] L.J. Farrugia. *J. Appl. Crystallogr.*, **30**, 565 (1997).
[30] M.J. Frisch, G.W. Trucks, H.B. Schlegel, G.E. Scuseria, M.A. Robb, J.R. Cheeseman, J.A. Montgomery, Jr., T. Vreven, K.N. Kudin, J.C. Burant, J.M. Millam, S.S. Iyengar, J. Tomasi, V. Barone, B. Mennucci, M. Cossi, G. Scalmani, N. Rega, G.A. Petersson, H. Nakatsuji, M. Hada, M. Ehara, K. Toyota, R. Fukuda, J. Hasegawa, M. Ishida, T. Nakajima, Y. Honda, O. Kitao, H. Nakai, M. Klene, X. Li, J.E. Knox, H.P. Hratchian, J.B. Cross, C. Adamo, J. Jaramillo, R. Gomperts, R.E. Stratmann, O. Yazyev, A.J. Austin, R. Cammi, C. Pomelli, J.W. Ochterski, P.Y. Ayala, K. Morokuma, G.A. Voth, P. Salvador, J.J. Dannenberg, V.G. Zakrzewski, S. Dapprich, A.D. Daniels, M.C. Strain, O. Farkas, D.K. Malick, A.D. Rabuck, K. Raghavachari, J.B. Foresman, J.V. Ortiz, Q. Cui, A.G. Baboul, S. Clifford, J. Cioslowski, B.B. Stefanov, G. Liu, A. Liashenko, P. Piskorz, I. Komaromi, R.L. Martin, D.J. Fox, T. Keith, M.A. Al-Laham, C.Y. Peng, A. Nanayakkara, M. Challacombe, P.M.W. Gill, B. Johnson, W. Chen, M.W. Wong, C. Gonzalez, J.A. Pople. *Gaussian 03, Revision A.1*, Gaussian, Inc., Pittsburgh, PA (2003).
[31] A.D. Becke. *Phys. Rev. A*, **38**, 3098 (1988).
[32] C. Lee, W. Yang, R.G. Parr. *Phys. Rev. B*, **37**, 785 (1988).
[33] R. Ditchfield, W.J. Hehre, J.A. Pople. *J. Chem. Phys.*, **54**, 724 (1971).
[34] W. Yang, W.J. Mortier. *J. Am. Chem. Soc.*, **108**, 5708 (1986).
[35] P.P. Chakrabarty, D. Biswas, S. García-Granda, A.D. Jana, S. Saha. *Polyhedron*, **35**, 108 (2012).
[36] S. Koner, S. Saha, K.-I. Okamoto, J.-P. Tuchagues. *Inorg. Chem.*, **42**, 4668 (2003).
[37] A. Biswas, M.G.B. Drew, C.J. Gómez-Garćia, A. Ghosh. *Inorg. Chem.*, **49**, 8155 (2010).
[38] J.A. Platts, S.T. Howard, K. Woźniak. *Chem. Phys. Lett.*, **232**, 479 (1995).
[39] D. Biswas, P.P. Chakrabarty, S. Saha, A.D. Jana, D. Schollmeyer, S. García-Granda. *Inorg. Chim. Acta*, **408**, 172 (2013).
[40] O. Kahn. *Molecular Magnetism*, VCH Publishers, New York (1993).
[41] B. Bleaney, K.D. Bowers. *Proc. Roy. Soc. A*, **214**, 451 (1952).
[42] C. Adhikary, S. Koner. *Coord. Chem. Rev.*, **254**, 2933 (2010) and references cited therein.
[43] M. Montazerozohori, K. Nozarian, H.R. Ebrahimi. *J. Spectrosc.,* **2013**, 1–9 (2013), Article ID 718149.
[44] Z. Xu, X. Qian. *Org. Lett.*, **7**, 3029 (2005).